Correlated Detection of sub-mHz Gravitational Waves by Two Optical-Fiber Interferometers

Reginald T. Cahill* and Finn Stokes†

*School of Chemistry, Physics and Earth Sciences, Flinders University, Adelaide 5001, Australia
E-mail: Reg.Cahill@flinders.edu.au
†Australian Science and Mathematics School, Flinders University, Adelaide 5001, Australia
E-mail: Finn.Stokes@gmail.com

Results from two optical-fiber gravitational-wave interferometric detectors are reported. The detector design is very small, cheap and simple to build and operate. Using two detectors has permitted various tests of the design principles as well as demonstrating the first simultaneous detection of correlated gravitational waves from detectors spatially separated by 1.1 km. The frequency spectrum of the detected gravitational waves is sub-mHz with a strain spectral index $a = -1.4 \pm 0.1$. As well as characterising the wave effects the detectors also show, from data collected over some 80 days in the latter part of 2007, the dominant earth rotation effect and the earth orbit effect. The detectors operate by exploiting light speed anisotropy in optical-fibers. The data confirms previous observations of light speed anisotropy, earth rotation and orbit effects, and gravitational waves.

1 Introduction

Results from two optical-fiber gravitational-wave interferometric detectors are reported. Using two detectors has permitted various tests of the design principles as well as demonstrating the first simultaneous detection of correlated gravitational waves from detectors spatially separated by 1.1 km. The frequency spectrum of the detected gravitational waves is sub-mHz. As well as charactersing the wave effects the detectors also show, from data collected over some 80 days in the latter part of 2007, the dominant earth rotation effect and the earth orbit effect. The detectors operate by exploiting light speed anisotropy in optical-fibers. The data confirms previous observations [1–4, 6–10] of light speed anisotropy, earth rotation and orbit effects, and gravitational waves. These observations and experimental techniques were first understood in 2002 when the Special Relativity effects and the presence of gas were used to calibrate the Michelson interferometer in gas-mode; in vacuum-mode the Michelson interferometer cannot respond to light speed anisotropy [11, 12], as confirmed in vacuum resonant-cavity experiments, a modern version of the vacuum-mode Michelson interferometer [13]. The results herein come from improved versions of the prototype optical-fiber interferometer detector reported in [9], with improved temperature stabilisation and a novel operating technique where one of the interferometer arms is orientated with a small angular offset from the local meridian. The detection of sub-mHz gravitational waves dates back to the pioneering work of Michelson and Morley in 1887 [1], as discussed in [16], and detected again by Miller [2] also using a gas-mode Michelson interferometer, and by Torr and Kolen [6], DeWitte [7] and Cahill [8] using RF waves in coaxial cables, and by Cahill [9] and herein using an optical-fiber interfer-

ometer design, which is very much more sensitive than a gas-mode interferometer, as discussed later.

It is important to note that the repeated detection, over more than 120 years, of the anisotropy of the speed of light is not in conflict with the results and consequences of Special Relativity (SR), although at face value it appears to be in conflict with Einstein's 1905 postulate that the speed of light is an invariant in vacuum. However this contradiction is more apparent than real, for one needs to realise that the space and time coordinates used in the standard SR Einstein formalism are *constructed* to make the speed of light invariant wrt those special coordinates. To achieve that observers in relative motion must then relate their space and time coordinates by a Lorentz transformation that mixes space and time coordinates — but this is only an artifact of this formalism*. Of course in the SR formalism one of the frames of reference could have always been designated as the observable one. Such an ontologically real frame of reference, only in which the speed of light is isotropic, has been detected for over 120 years, yet ignored by mainstream physics. The problem is in not clearly separating a very successful mathematical formalism from its predictions and experimental tests. There has been a long debate over whether the Lorentz 3-space *and* time interpretation or the Einstein spacetime interpretation of observed SR effects is preferable or indeed even experimentally distinguishable.

What has been discovered in recent years is that a dynamical structured 3-space exists, so confirming the Lorentz interpretation of SR, and with fundamental implications for physics — for physics failed to notice the existence of the

---

*Thus the detected light speed anisotropy does not indicate a breakdown of Lorentz symmetry, contrary to the aims but not the outcomes of [13].
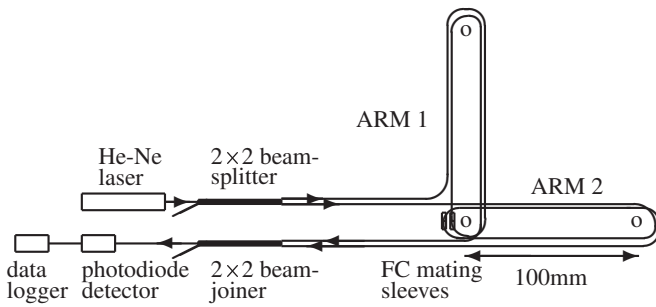
Fig. 1: Schematic layout of the interferometric optical-fiber light-speed anisotropy/gravitational wave detector. Actual detector is shown in Fig. 2. Coherent 633 nm light from the a He-Ne Laser is split into two lengths of single-mode polarisation preserving fibers by the 2×2 beam splitter. The two fibers take different directions, ARM1 and ARM2, after which the light is recombined in the 2×2 beam joiner, in which the phase differences lead to interference effects that are indicated by the outgoing light intensity, which is measured in the photodiode detector/amplifier (Thorlabs PDA36A or PDA36A-EC), and then recorded in the data logger. In the actual layout the fibers make two loops in each arm, but with excess lengths wound around one arm (not shown) — to reduce effective fiber lengths so as to reduce sensitivity. The length of one straight section is 100 mm, which is the center to center spacing of the plastic turners, having diameter = 52 mm, see Fig. 2. The relative travel times, and hence the output light intensity, are affected by the varying speed and direction of the flowing 3-space, by affecting differentially the speed of the light, and hence the net phase difference between the two arms.

Fig. 2: Photograph of a detector showing the optical fibers forming the two orthogonal arms. See Fig. 1 for the schematic layout. The 2×2 beam splitter and joiner (Thorlabs FC632-50B-FC) are the two small stainless steel cylindrical tubes. The two FC to FC mating sleeves (Thorlabs ADAFC1) are physically adjacent. The overall dimensions of the metal base plate are 160×160 mm. The 2×2 splitter and joiner each have two input and two output fibers, with one not used. Arm 2 is folded over the splitter and joiner, compared to the schematic layout. The interferometer shown costs approximately $400.

main *constituent* defining the universe, namely a dynamical 3-space, with quantum matter and EM radiation playing a minor role. This dynamical 3-space provides an explanation for the success of the SR Einstein formalism. It also provides a new account of gravity, which turns out to be a quantum effect [17], and of cosmology [16, 18–20], doing away with the need for dark matter and dark energy.

2 Dynamical 3-space and gravitational waves

Light-speed anisotropy experiments have revealed that a dynamical 3-space exists, with the speed of light being c, in vacuum, only wrt to this space: observers in motion "through" this 3-space detect that the speed of light is in general different from c, and is different in different directions*. The dynamical equations for this 3-space are now known and involve a velocity field $\mathbf{v}(\mathbf{r}, t)$, but where only relative velocities are observable locally — the coordinates $\mathbf{r}$ are relative to a non-physical mathematical embedding space. These dynamical equations involve Newton's gravitational constant G and the fine structure constant α. The discovery of this dynamical 3-space then required a generalisation of the Maxwell, Schrödinger and Dirac equations. The wave effects already detected correspond to fluctuations in the 3-space velocity field $\mathbf{v}(\mathbf{r}, t)$, so they are really 3-space turbulence or wave effects. However they are better known, if somewhat inappropriately, as "gravitational waves" or "ripples" in "spacetime". Because the 3-space dynamics gives a deeper understanding of the spacetime formalism we now know that the metric of the induced spacetime, merely a mathematical construct having no ontological significance, is related to $\mathbf{v}(\mathbf{r}, t)$ according to [16, 18, 20]

$$ds^2 = dt^2 - \frac{(d\mathbf{r} - \mathbf{v}(\mathbf{r}, t)dt)^2}{c^2} = g_{\mu\nu}dx^\mu dx^\nu. \quad (1)$$

The gravitational acceleration of matter, and of the structural patterns characterising the 3-space, are given by [16, 17]

$$\mathbf{g} = \frac{\partial \mathbf{v}}{\partial t} + (\mathbf{v} \cdot \nabla)\mathbf{v} \quad (2)$$

and so fluctuations in $\mathbf{v}(\mathbf{r}, t)$ may or may not manifest as a gravitational force. The general characteristics of $\mathbf{v}(\mathbf{r}, t)$ are now known following the detailed analysis of the experiments noted above, namely its average speed, and removing the earth orbit effect, is some 420±30 km/s, from direction RA = 5.5±2$^{\text{hr}}$, Dec = 70±10° S — the center point of the Miller data in Fig. 12b, together with large wave/turbulence effects. The magnitude of this turbulence depends on the timing resolution of each particular experiment, and here we

---

*Many failed experiments supposedly designed to detect this anisotropy can be shown to have design flaws.

Fig. 3: (a) Detector 1 (D1) is located inside a sealed air-filled bucket inside an insulated container (blue) containing some 90 kg of water for temperature stabilisation. This detector, in the School of Chemistry, Physics and Earth Sciences, had an orientation of 5° anti-clockwise to the local meridian. Cylindrical He-Ne laser (Melles-Griot 0.5 mW 633 nm 05-LLR-811-230) is located on LHS of bench, while data logger is on RHS. Photodiode detector/pre-amplifier is located atop aluminium plate. (b) Detector 2 (D2) was located 1.1 km North of D1 in the Australian Science and Mathematics School. This detector had an orientation of 11° anti-clockwise to the local meridian. The data was logged on a PC running a PoScope USB DSO (PoLabs http://www.poscope.com).

characterise them at sub-mHz frequencies, showing that the fluctuations are very large, as also seen in [8].

3 Gravitational wave detectors

To measure $\mathbf{v}(\mathbf{r}, t)$ has been difficult until now. The early experiments used gas-mode Michelson interferometers, which involved the visual observation of small fringe shifts as the relatively large devices were rotated. The RF coaxial cable experiments had the advantage of permitting electronic recording of the RF travel times, over 500m [6] and 1.5 km [7], by means of two or more atomic clocks, although the experiment reported in [8] used a novel technique that enable the coaxial cable length to be reduced to laboratory size*.

---

*The calibration of this technique is at present not well understood in view of recent discoveries concerning the Fresnel drag effect in optical fibers.

Fig. 4: (a) Detectors are horizontally located inside an air-filled bucket. The plastic bag reduces even further any air movements, and thus temperature differentials. The blue crystals are silica gel to reduce moisture. (b) Bucket located inside and attached to bottom of the insulated container prior to adding water to the container.

The new optical-fiber detector design herein has the advantage of electronic recording as well as high precision because the travel time differences in the two orthogonal fibers employ light interference effects, but with the interference effects taking place in an optical fiber beam-joiner, and so no optical projection problems arise. The device is very small, very cheap and easily assembled from readily available opto-electronic components. The schematic layout of the detector is given in Fig. 1, with a detailed description in the figure caption. The detector relies on the phenomenon where the 3-space velocity $\mathbf{v}(\mathbf{r}, t)$ affects differently the light travel times in the optical fibers, depending on the projection of $\mathbf{v}(\mathbf{r}, t)$ along the fiber directions. The differences in the light travel times are measured by means of the interference effects in the beam joiner. The difference in travel times is given by

$$\Delta t = k^2 \, \frac{L v_P^2}{c^3} \cos(2\theta), \tag{3}$$

where
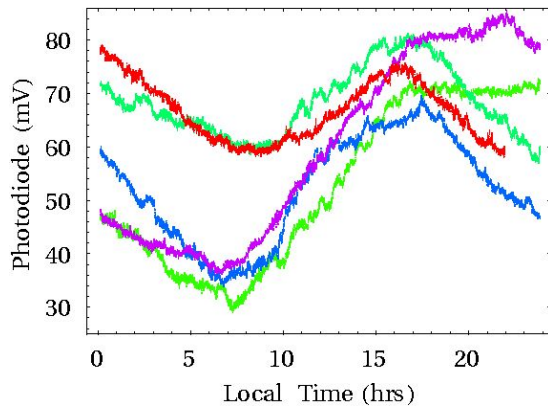
$$k^2 = \frac{(n^2 - 1)(2 - n^2)}{n}$$

Fig. 5: D1 photodiode output voltage data (mV), recorded every 5 secs, from 5 successive days, starting September 22, 2007, plotted against local Adelaide time (UT = local time + 9.5 hrs). Day sequence is indicated by increasing hue. Dominant minima and maxima is earth rotation effect. Fluctuations from day to day are evident as are fluctuations during each day — these are caused by wave effects in the flowing space. Changes in RA cause changes in timing of min/max, while changes in magnitude are caused by changes in declination and/or speed. Blurring effect is caused by laser noise. Same data is plotted sequentially in Fig. 7a.

is the instrument calibration constant, obtained by taking account of the three key effects: (i) the different light paths, (ii) Lorentz contraction of the fibers, an effect depending on the angle of the fibers to the flow velocity, and (iii) the refractive index effect, including the Fresnel drag effect. Only if $n \neq 1$ is there a net effect, otherwise when $n = 1$ the various effects actually cancel. So in this regard the Michelson interferometer has a serious design flaw. This problem has been overcome by using optical fibers. Here $n = 1.462$ at 633 nm is the effective refractive index of the single-mode optical fibers (Fibercore SM600, temperature coefficient 5×10^{-2} fs/mm/C). Here $L \approx 200$ mm is the average effective length of the two arms, and $v_P(\mathbf{r}, t)$ is the projection of $\mathbf{v}(\mathbf{r}, t)$ onto the plane of the detector, and the angle θ is that of the projected velocity onto the arm.

The reality of the Lorentz contraction effect is experimentally confirmed by comparing the 2nd order in v/c Michelson gas-mode interferometer data, which requires account be taken of the contraction effect, with that from the 1st order in v/c RF coaxial cable travel time experiments, as in De-Witte [7], which does not require that the contraction effect be taken into account, to give comparable values for v.

For gas-mode Michelson interferometers $k^2 \approx n^2 - 1$, because then $n \approx 1^+$ is the refractive index of a gas. Operating in air, as for Michelson and Morley and for Miller, $n = 1.00029$, so that $k^2 = 0.00058$, which in particular means that the Michelson-Morley interferometer was nearly 2000 times less sensitive than assumed by Michelson, who used Newtonian physics to calibrate the interferometer — that analysis gives $k^2 = n^3 \approx 1$. Consequently the small fringe
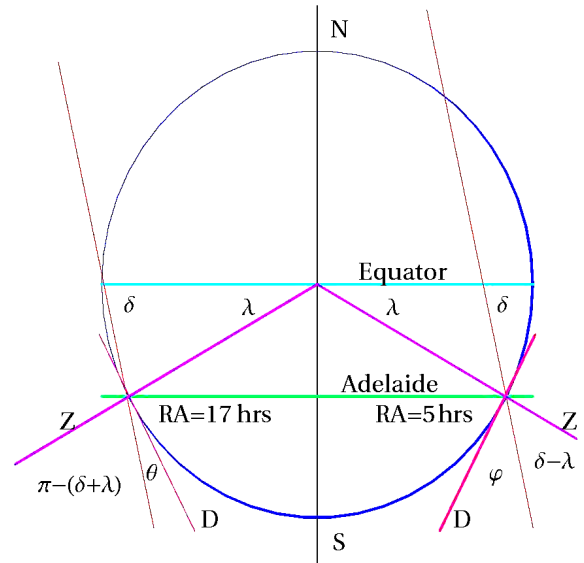

Fig. 6: Schematic of earth and spatial flow at approximate local sidereal times (RA) of 5 hrs and 17 hrs. The detector arms, D, of D1 and D2 are operated at small offset angles from the local meridian. The long straight lines indicate the spatial flow velocity vector, with declination δ. The large earth-rotation induced minima/maxima are caused by the inclination angle varying from a maximum ϕ to a minimum θ, respectively. Wave effects are changes in the velocity vector.

shifts observed by Michelson and Morley actually correspond to a light speed anisotropy of some 400 km/s, that is, the earth has that speed relative to the local dynamical 3-space. The dependence of k on n has been checked [11, 18] by comparing the air gas-mode data against data from the He gas-mode operated interferometers of Illingworth [3] and Joos [4].

The above analysis also has important implications for long-baseline terrestrial vacuum-mode Michelson interferometer gravitational wave detectors — they have a fundamental design flaw and will not be able to detect gravitational waves.

The interferometer operates by detecting changes in the travel time difference between the two arms, as given by (3). The cycle-averaged light intensity emerging from the beam joiner is given by

$$
\begin{aligned}
I(t) &\propto \left(\mathrm{Re}\left(\mathbf{E}_1 + \mathbf{E}_2 e^{i\omega(\tau + \Delta t)} \right) \right)^2 = \\
&= 2|\mathbf{E}|^2 \cos\left(\frac{\omega(\tau + \Delta t)}{2} \right)^2 \approx \\
&\approx a + b\Delta t.
\end{aligned} \tag{4}
$$

Here $\mathbf{E}_i$ are the electric field amplitudes and have the same value as the fiber splitter/joiner are 50%–50% types, and having the same direction because polarisation preserving fibers are used, ω is the light angular frequency and τ is a travel time difference caused by the light travel times not
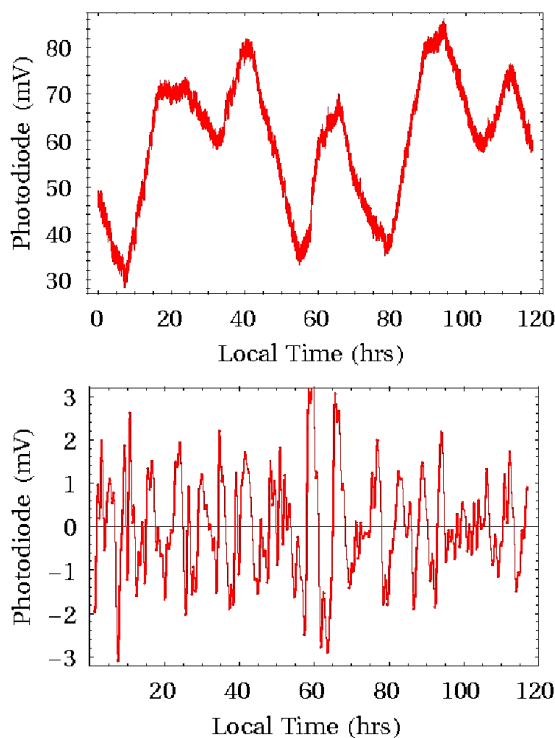
Fig. 7: (a) Plot of 5 days of data from Fig. 5 shown sequentially. The Fourier Transform of this data is shown in Fig. 12a. (b) Plot shows data after filtering out earth-rotation frequencies ($f < 0.025$ mHz) and laser noise frequencies ($f > 0.25$ mHz, $\mathrm{Log}_{10}[0.25] = -0.6$). This shows wave/turbulence effects. Note that the magnitude of the wave component of the signal is some 10% of full signal in this bandwidth.

being identical, even when $\Delta t = 0$, mainly because the various splitter/joiner fibers will not be identical in length. The last expression follows because Δt is small, and so the detector operates, hopefully, in a linear regime, in general, unless τ has a value equal to modulo(T), where T is the light period. The main temperature effect in the detector, so long as a temperature uniformity is maintained, is that τ will be temperature dependent. The temperature coefficient for the optical fibers gives an effective fractional fringe shift error of $\Delta\tau/T = 3 \times 10^{-2}$/mm/C, for each mm of length difference. The photodiode detector output voltage $V(t)$ is proportional to $I(t)$, and so finally linearly related to Δt. The detector calibration constants a and b depend on k, τ and the laser intensity and are unknown at present.

4 Data analysis

The data is described in detail in the figure captions.

- Fig. 5 shows 5 typical days of data exhibiting the earth-rotation effect, and also fluctuations during each day and from day to day, revealing dynamical 3-space turbulence — essentially the long-sort-for gravitational waves. It is now known that these gravitational waves

were first detected in the Michelson-Morley 1887 experiment [16], but only because their interferometer was operated in gas-mode. Fig. 12a shows the frequency spectrum for this data;

- Fig. 7b shows the gravitational waves after removing frequencies near the earth-rotation frequency. As discussed later these gravitational waves are predominately sub-mHz;

- Fig. 8 reports one of a number of key experimental tests of the detector principles. These show the two detector responses when (a) operating from the same laser source, and (b) with only D2 operating in interferometer mode. These reveal the noise effects coming from the laser in comparison with the interferometer signal strength. This gives a guide to the S/N ratio of these detectors;

- Fig. 9 shows two further key tests: 1st the time delay effect in the earth-rotation induced minimum caused by the detectors not being aligned NS. The time delay difference has the value expected. The 2nd effect is that wave effects are simultaneous, in contrast to the 1st effect. This is the first coincidence detection of gravitational waves by spatially separated detectors. Soon the separation will be extended to much larger distances;

- Figs. 10 and 11 show the data and calibration curves for the timing of the daily earth-rotation induced minima and maxima over an 80 day period. Because D1 is orientated away from the NS these times permit the determination of the Declination (Dec) and Right Ascension (RA) from the two running averages. That the running averages change over these 80 days reflects three causes (i) the sidereal time effect, namely that the 3-space velocity vector is related to the positioning of the galaxy, and not the Sun, (ii) that a smaller component is related to the orbital motion of the earth about the Sun, and (iii) very low frequency wave effects. This analysis gives the changing Dec and RA shown in Fig. 12b, giving results which are within $13°$ of the 1925/26 Miller results, and for the RA from the DeWitte RF coaxial cable results. Figs. 10a and 11a also show the turbulence/wave effects, namely deviations from the running averages;

- Fig. 12a shows the frequency analysis of the data. The fourier amplitudes, which can be related to the strain $h = v^2/2c^2$, decrease as f^a where the strain spectral index has the value $a = -1.4 \pm 0.1$, after we allow for the laser noise.

5 Conclusions

Sub-mHz gravitational waves have been detected and partially characterised using the optical-fiber version of a Michelson interferometer. The waves are relatively large and were
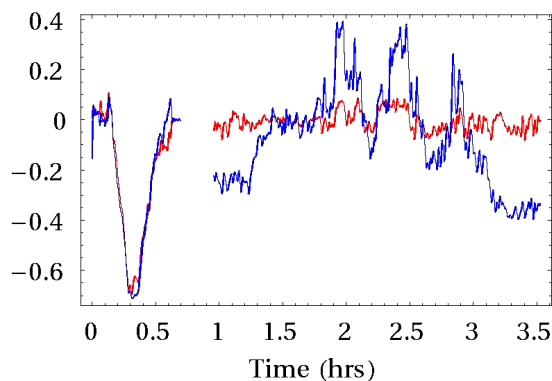
Fig. 8: Two tests of the detectors. (a) The left plot shows data from D1 and D2 when co-located, parallel and operating from the same laser. The data from one has been rescaled to match the data from the other, as they have different calibrations. Both detectors show a simultaneous gravitational wave pulse of duration ≈ 0.5 hrs. (b) The right plot shows data from D2 (blue) and from a direct feed of the common laser source to the photodiode detector of D1 (red), i.e bypassing the D1 interferometer. This data has been rescaled so that high frequency components have the same magnitude, to compensate for different feed amplitudes. The laser-only signal (red) shows the amplitude and frequency noise level of the laser. The signal from D2 (blue) shows the same noise effects, but with additional larger variations — these are wave effects detected by D2 operating in interferometer mode. This data shows that the laser noise is dominant above approximately 1 mHz.

first detected, though not recognised as such, by Michelson and Morley in 1887. Since then another 6 experiments [2,6–9], including herein, have confirmed the existence of this phenomenon. Significantly three different experimental techniques have been employed, all giving consistent results. In contrast vacuum-mode Michelson interferometers, with mechanical mirror support arms, cannot detect this phenomenon due to a design flaw. A complete characterisation of the waves requires that the optical-fiber detector be calibrated for speed, which means determining the parameter b in (4). Then it will be possible to extract the wave component of $\mathbf{v}(\mathbf{r}, \mathbf{t})$ from the average, and so identify the cause of the turbulence/wave effects. A likely candidate is the in-flow of 3-space into the Milky Way central super-massive black hole — this in-flow is responsible for the high, non-Keplerian, rotation speeds of stars in the galaxy.

The detection of the earth-rotation, earth-orbit and gravitational waves, and over a long period of history, demonstrate that the spacetime formalism of Special Relativity has been very misleading, and that the original Lorentz formalism is the appropriate one; in this the speed of light is not an invariant for all observers, and the Lorentz-Fitzgerald length contraction and the Lamor time dilation are real physical effects on rods and clocks in motion through the dynamical 3-space, whereas in the Einstein formalism they are transferred and attributed to a perspective effect of spacetime, which we now recognise as having no ontological significance — merely a
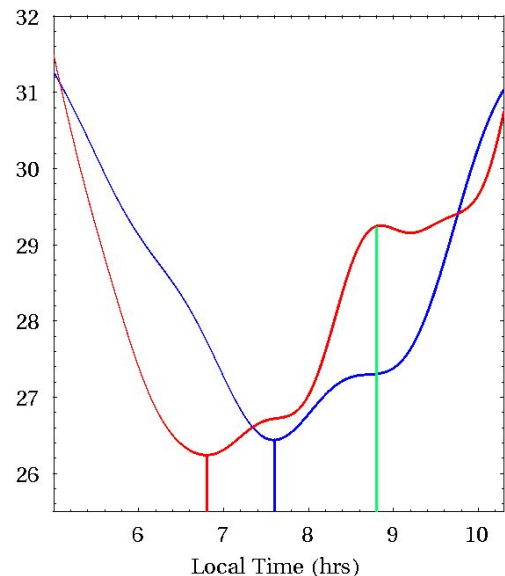

Fig. 9: Photodiode data (mV) on October 4, 2007, from detectors D1 (red plot) and D2 (blue plot) operating simultaneously with D2 located 1.1 km due north of D1. A low-pass FFT filter ($f \leqslant 0.25$ mHz, $\mathrm{Log}_{10}[f(\mathrm{mHz})] \leqslant -0.6$) was used to remove laser noise. D1 arm is aligned $5°$ anti-clockwise from local meridian, while D2 is aligned $11°$ anti-clockwise from local meridian. The alignment offset between D1 and D2 causes the dominant earth-rotation induced minima to occur at *different* times, with that of D2 at $t = 7.6$ hrs *delayed* by 0.8 hrs relative to D1 at $t = 6.8$ hrs, as expected from Figs. 10b and 11b for Dec $= 77°$. This is a fundamental test of the detection theory and of the phenomena. As well the data shows a *simultaneous* sub-mHz gravitational wave correlation at $t \approx 8.8$ hrs and of duration ≈ 1 hr. This is the first observed correlation for spatially separated gravitational wave detectors. Two other wave effects (at $t \approx 6.5$ hrs in D2 and $t \approx 7.3$ hrs in D1) seen in one detector are masked by the stronger earth-rotation induced minimum in the other detector.

mathematical construct, and in which the invariance of the speed of light is definitional — not observational.

References

1. Michelson A.A. and Morley E.W. *Am. J. Sc.*, 1887, v. 34, 333–345.

2. Miller D.C. *Rev. Mod. Phys.*, 1933, v. 5, 203–242.

3. Illingworth K.K. *Phys. Rev.*, 1927, v. 3, 692–696.

4. Joos G. *Ann. d. Physik*, 1930, v. 7, 385.

5. Jaseja T.S. *et al. Phys. Rev. A*, 1964, v. 133, 1221.

6. Torr D.G. and Kolen P. In: *Precision Measurements and Fundamental Constants*, Ed. by Taylor B.N. and Phillips W.D., *Natl. Bur. Stand. (U.S.), Spec. Pub.*, 1984, v. 617, 675.

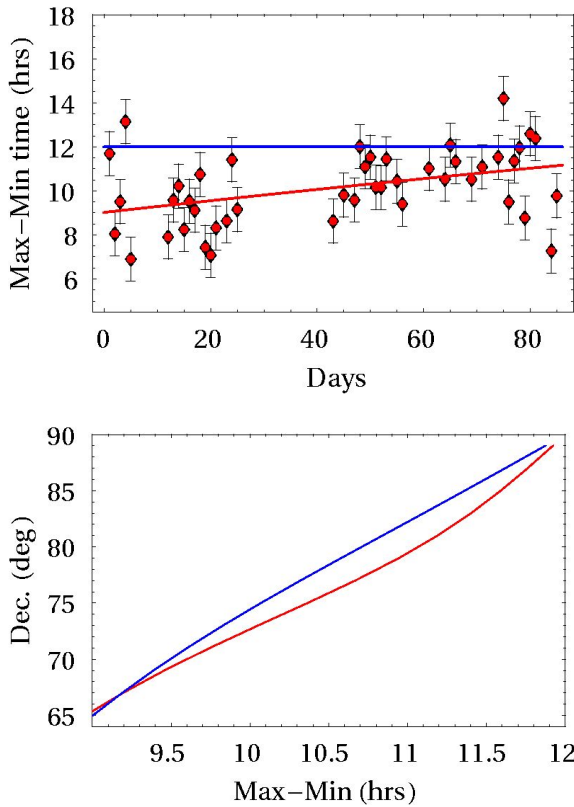7. Cahill R.T. The Roland DeWitte 1991 experiment. *Progress in Physics*, 2006, v. 3, 60–65.

Fig. 10: (a) Time differences between maxima and minima each day from D1, from September 22 to December 16, 2007. Some days are absent due to data logger malfunction. The red curve shows a quadratic best-fit running average. If the detector arm was orientated along the meridian and there were no wave effects then one would see the horizontal line (blue) at 12 hrs. The data shows, however, that the running average has a time varying measure, from 9 hrs to 11 hrs over these days, caused by the orbital motion of the earth about the sun. Wave-effect fluctuations from day to day are also evident. This data in conjunction with the calibration curve in (b) permits a determination of the approximate Declination each day, which is used in the plot shown in Fig. 12b. (b) Declination calibration curve for D1 (red) and D2 (blue). From the orientation of the detector, with an offset angle of 5° for D1 anti-clockwise from the local meridian and 11° for D2 anti-clockwise from the local meridian, and the latitude of Adelaide, the offset angle causes the time duration between a minimum and a maximum to be different from 12 hrs, ignoring wave effects. In conjunction with the running average in Fig. 10a an approximate determination of the Declination on each day may be made without needing to also determine the RA and speed.
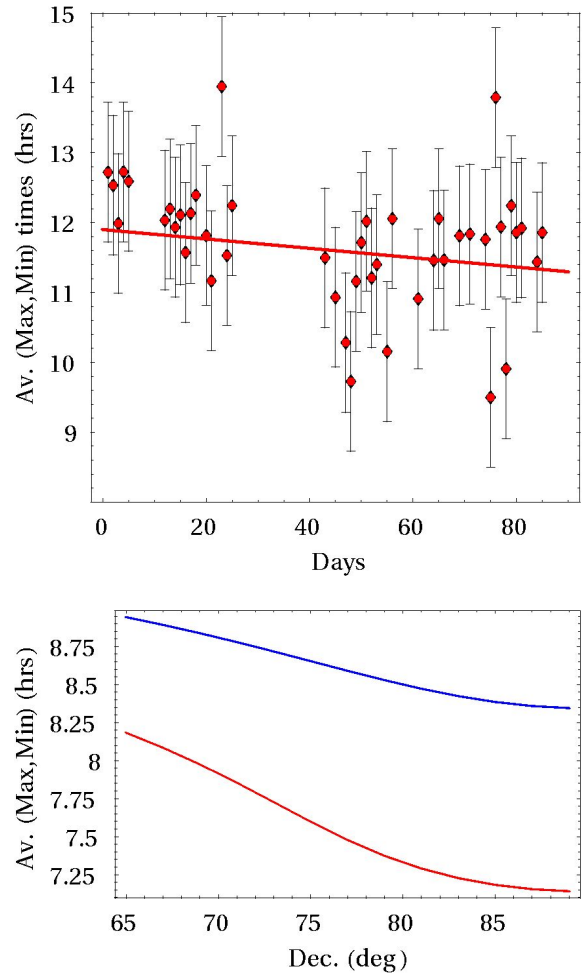

Fig. 11: (a) Time of average of minimum and maximum for each day. The linear best-fit line shows the trend line. Wave effects are again very evident. The decreasing trend line is cause by a combination of the sidereal effect, the earth orbit effect and very low frequency waves. This data may be used to determine the approximate RA for each day. However a correction must be applied as the arm offset angle affects the determination. (b) RA calibration curve for D1 (red) and D2 (blue). The detector offset angles cause the timing of the mid-point between the minima and maxima, ignoring wave effects, to be delayed in time, beyond the 6 hrs if detector were aligned NS. So, for example, if the Declination is found to be 70°, then this calibration curve gives 8 hrs for D1. This 8 hrs is then subtracted from the time in (a) to give the approximate true local time for the minimum to occur, which then permits computation of the RA for that day.
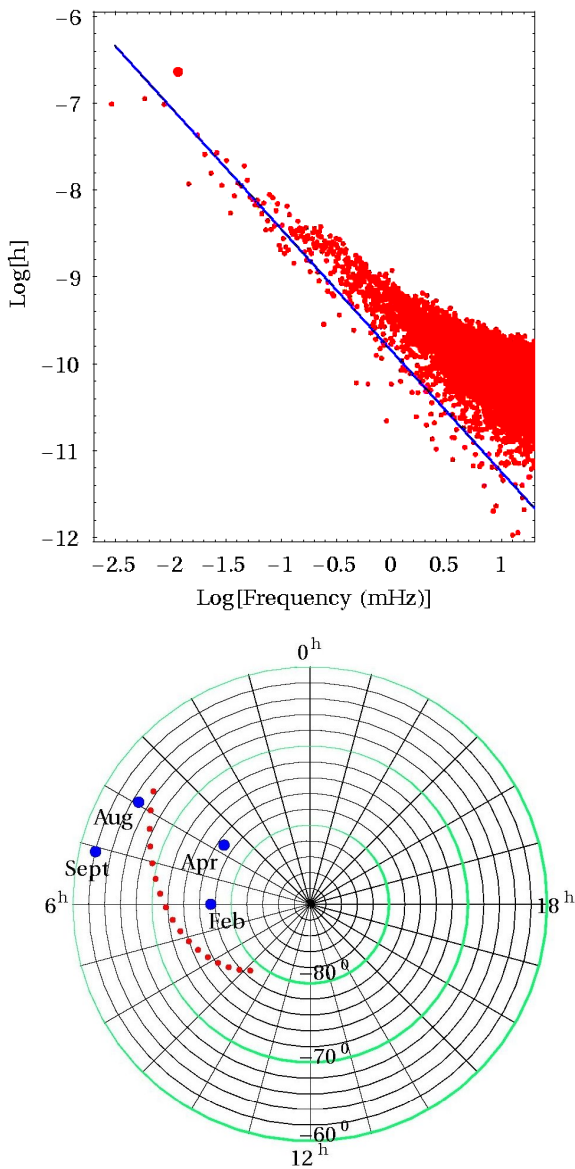
8. Cahill R.T. A new light-speed anisotropy experiment: absolute motion and gravitational waves detected. *Progress in Physics*, 2006, v. 4, 73–92.

9. Cahill R.T. Optical-fiber gravitational wave detector: dynamical 3-space turbulence detected. *Progress in Physics*, 2007, v. 4, 63–68.

10. Munéra H.A., *et al.* In: *Proceedings of SPIE*, v. 6664, K1–K8, 2007, Ed. by Roychoudhuri C. *et al.*

11. Cahill R.T. and Kitto K. Michelson-Morley experiments revisited. *Apeiron*, 2003, v. 10(2), 104–117.

12. Cahill R.T. The Michelson and Morley 1887 experiment and the discovery of absolute motion. *Progress in Physics*, 2005, v. 3, 25–29.

13. Braxmaier C., *et al. Phys. Rev. Lett.*, 2002, v. 88, 010401; Müller H., *et al. Phys. Rev. D*, 2003, v. 68, 116006-1-17; Müller H., *et al. Phys. Rev. D*, 2003, v. 67, 056006; Wolf P., *et al. Phys. Rev. D*, 2004, v. 70, 051902-1-4; Wolf P., *et al. Phys. Rev. Lett.*, 2003, v. 90, no. 6, 060402; Lipa J.A., *et al. Phys. Rev. Lett.*, 2003, v. 90, 060403.

14. Levy J. From Galileo to Lorentz ... and beyond. *Apeiron*, Montreal, 2003.

15. Guerra V. and de Abreu R. Relativity: Einstein's lost frame. Extramuros, 2005.

16. Cahill R.T. Dynamical 3-space: a review. To be pub. in: *Physical Interpretations of Relativity Theory*, arXiv: 0705.4146.

17. Cahill R.T. Dynamical fractal 3-space and the generalised Schrödinger equation: Equivalence Principle and vorticity effects. *Progress in Physics*, 2006, v. 1, 27–34.

18. Cahill R.T. Process physics: from information theory to quantum space and matter. Nova Science Pub., New York, 2005.

19. Cahill R.T. Dynamical 3-space: supernovae and the Hubble expansion — the older Universe without dark energy. *Progress in Physics*, 2007, v. 4, 9–12.

20. Cahill R.T. A quantum cosmology: no dark matter, dark energy nor accelerating Universe. arXiv: 0709.2909.

Fig. 12: (a) Log-Log plot of the frequency spectrum $|h(f)|$ of the data from the five days shown in Fig. 7a. $h(f)$ is the strain $v^2/2c^2$ at frequency f, normalised to $v = 400$ km/s at the 24 hr frequency. The largest component (large red point) is the 24 hr earth rotation frequency. The straight line (blue) is a trend line that suggests that the signal has two components — one indicated by the trend line having the form $|h(f)| \propto f^a$ with strain spectral index $a = -1.4 \pm 0.1$, while the second component, evident above 1 mHz, is noise from the laser source, as also indicated by the data in Fig. 8. (b) Southern celestial sphere with RA and Dec shown. The 4 blue points show the results from Miller [2] for four months in 1925/1926. The sequence of red points show the daily averaged RA and Dec as determined from the data herein for every 5 days. The 2007 data shows a direction that moves closer to the south celestial pole in late December than would be indicated by the Miller data. The new results differ by 10° to 13° from the corresponding Miller data points (the plot exaggerates angles). The wave effects cause the actual direction to fluctuate from day to day and during each day.